Supporting Information

Synthesis, Morphology, and Electrical Memory Application of Oligosaccharide-based Block Copolymers with π-Conjugated Pyrene Moiety and Their Supramolecules

Han-Sheng Sun,[1] Yougen Chen,[2] Wen-Ya Lee,[3] Yu-Cheng Chiu,[1] Takuya Isono,[2] Toshifumi Satoh,[2,*] Toyoji Kakuchi,[2,*] and Wen-Chang Chen[1,*]

[1]Department of Chemical Engineering, National Taiwan University, Taipei, Taiwan, 10617

[2]Division of Biotechnology and Macromolecular Chemistry, Faculty of Engineering Hokkaido University, Sapporo, 060-8628, Japan

[3]Department of Chemical Engineering and Biotechnology, National Taipei University of Technology, Taipei, Taiwan, 10608

*To whom all correspondence should be addressed: Tel:+886-2-23628398. E-mail: chenwc@ntu.edu.tw (W.C.C.); Tel & Fax:+81-11-706-6602. E-mail: kakuchi@poly-bm.eng.hokudai.jp (T.K.), satoh@poly-bm.eng.hokudai.ac.jp (T.S.)

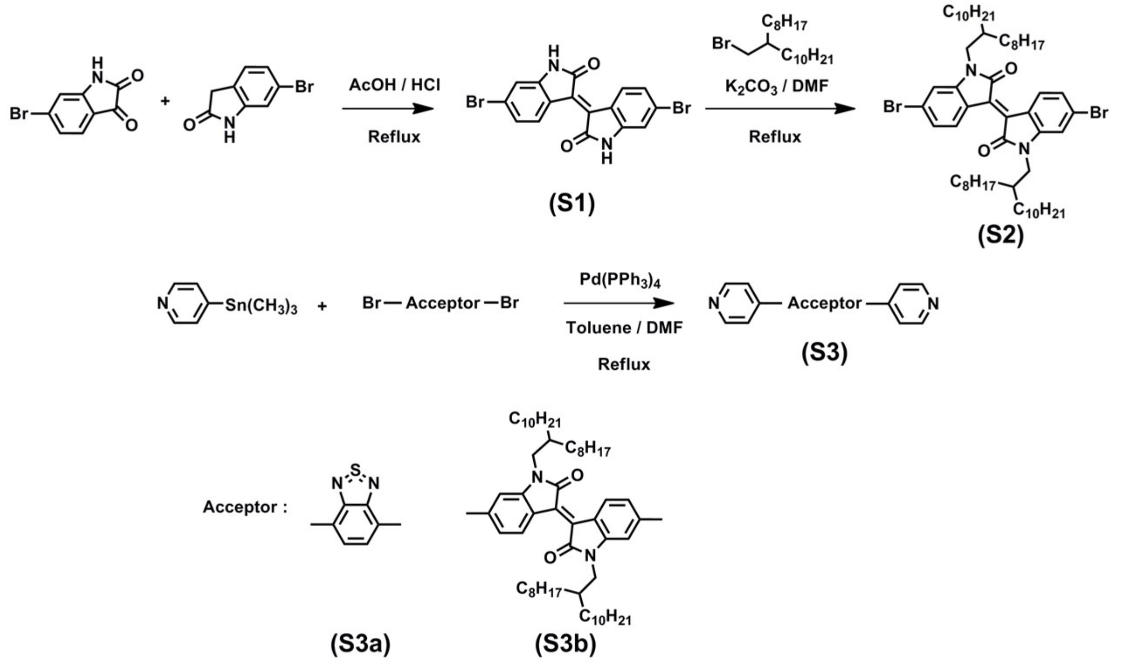

Scheme S1. The synthetic route for 4Py-Acceptor-4Py.

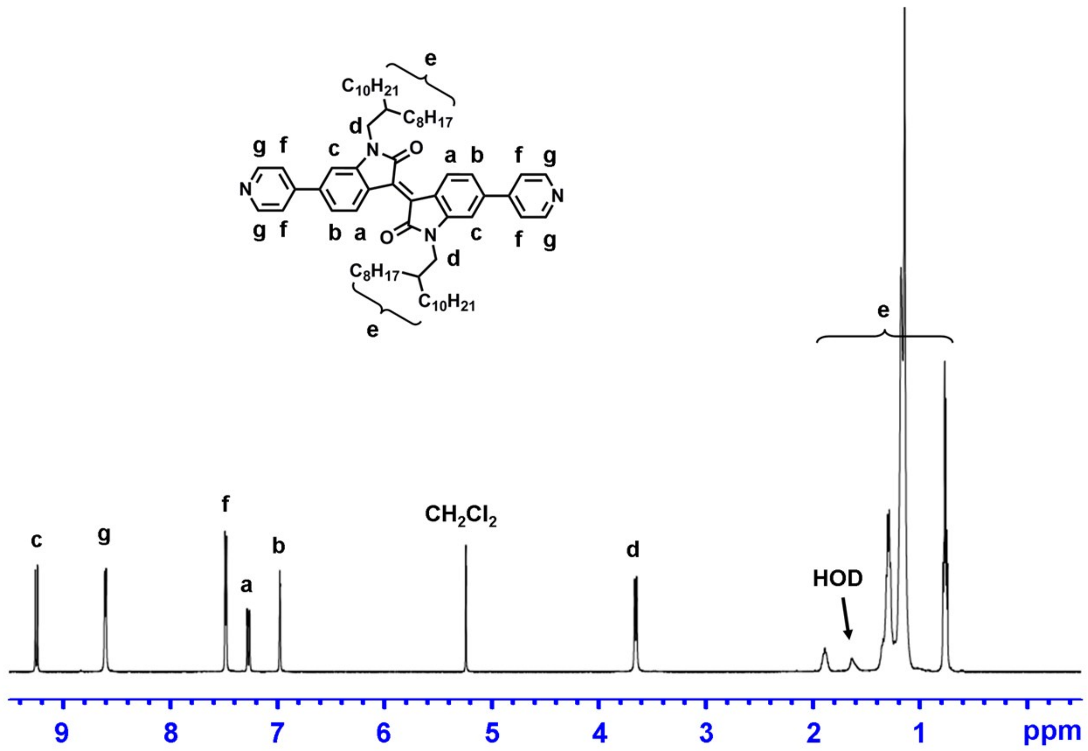

Fig. S1 [1]H NMR spectrum of 6,6'-di(4-pyridyl)-*N,N'*-bis(2-octyldodecyl)-isoindigo in CD_2Cl_2.

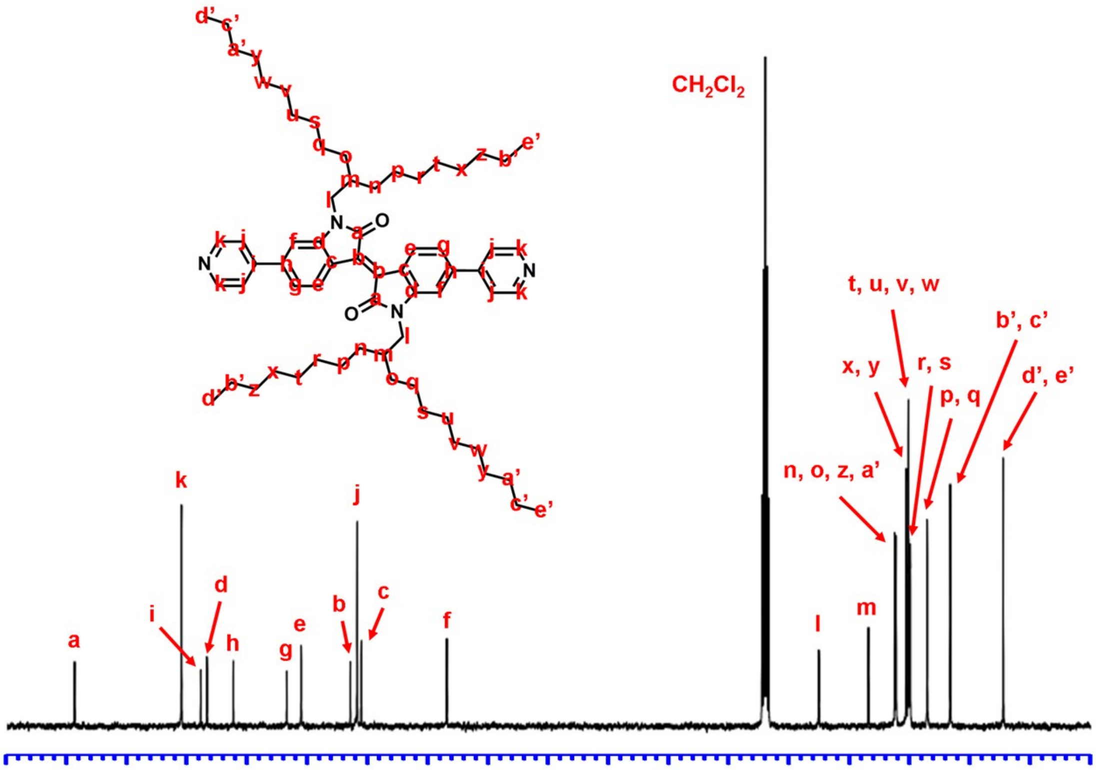

Fig. S2 [13]C NMR spectrum of 6,6'-di(4-pyridyl)-*N,N'*-bis(2-octyldodecyl)-isoindigo in CD_2Cl_2.

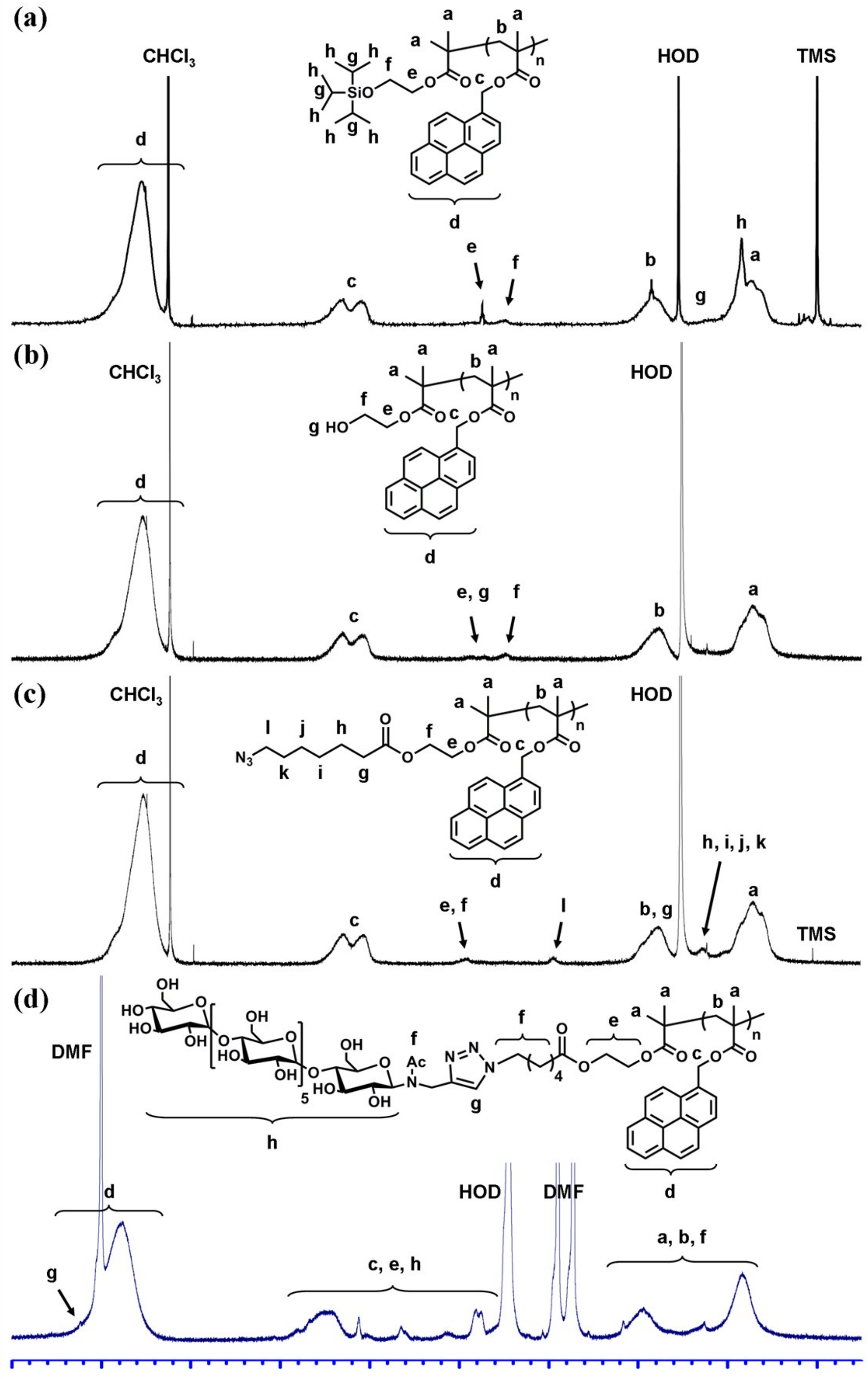

Fig. S3 ^{1}H NMR spectra of (a) PPyMA$_{20}$-OSi^{i}Pr$_3$ in CDCl$_3$, (b) PPyMA$_{20}$-OH in CDCl$_3$, (c) PPyMA$_{20}$-N$_3$ in CDCl$_3$, and (d) MH-*b*-PPyMA$_{20}$ diblock copolymer in DMF-d_7.

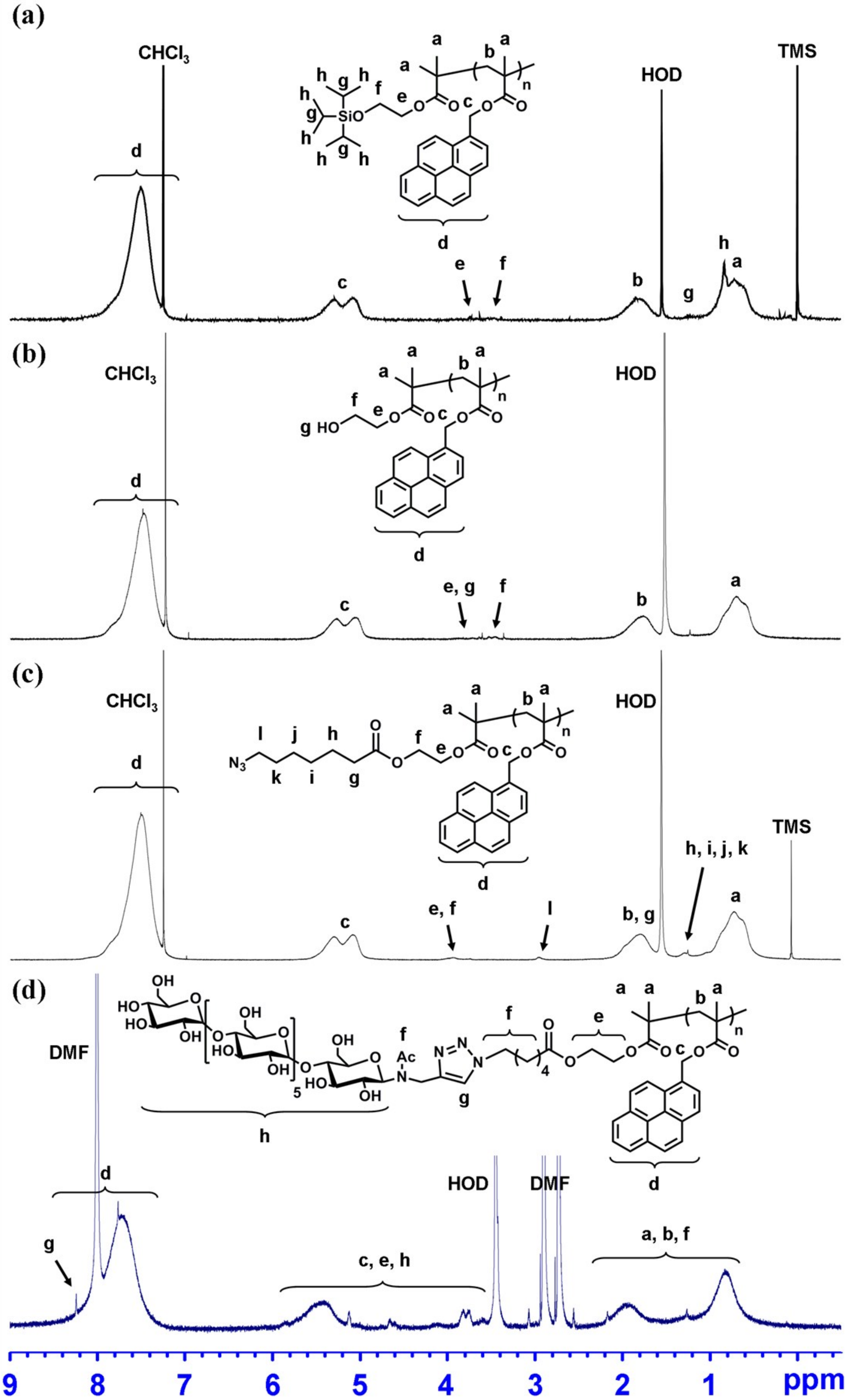

Fig. S4 [1]H NMR spectra of (a) $PPyMA_{40}$-$OSi^{i}Pr_3$ in $CDCl_3$, (b) $PPyMA_{40}$-OH in $CDCl_3$, (c) $PPyMA_{40}$-N_3 in $CDCl_3$, and (d) MH-*b*-$PPyMA_{40}$ diblock copolymer in DMF-d_7.

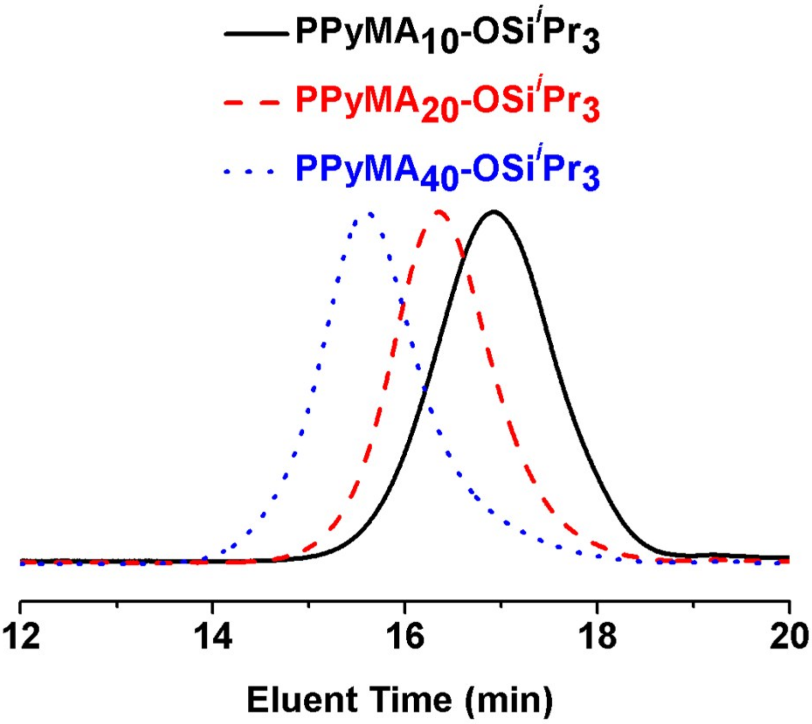

Fig. S5 GPC traces of the triisopropylsilyloxy-terminated PPyMA$_n$ (PPyMA$_n$-OSi^{i}Pr$_3$, n = 10, 20 and 40) homopolymers.

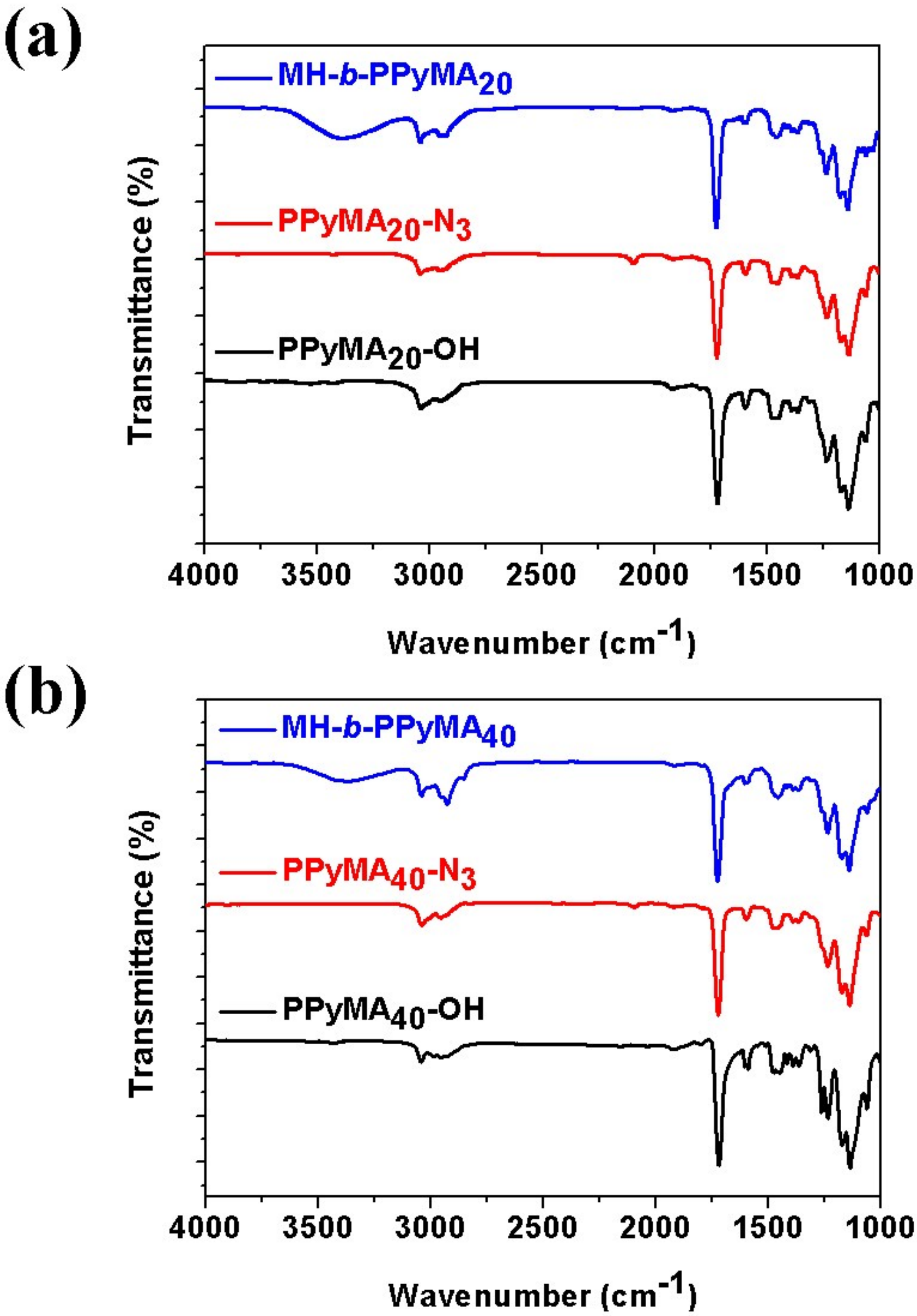

Fig. S6 FTIR spectra of (a) the hydroxyl- and azido-terminated $PPyMA_{20}$ homopolymers and MH-*b*-$PPyMA_{20}$ diblock copolymer, and (b) the hydroxyl- and azido-terminated $PPyMA_{40}$ homopolymers and MH-*b*-$PPyMA_{40}$ diblock copolymer.

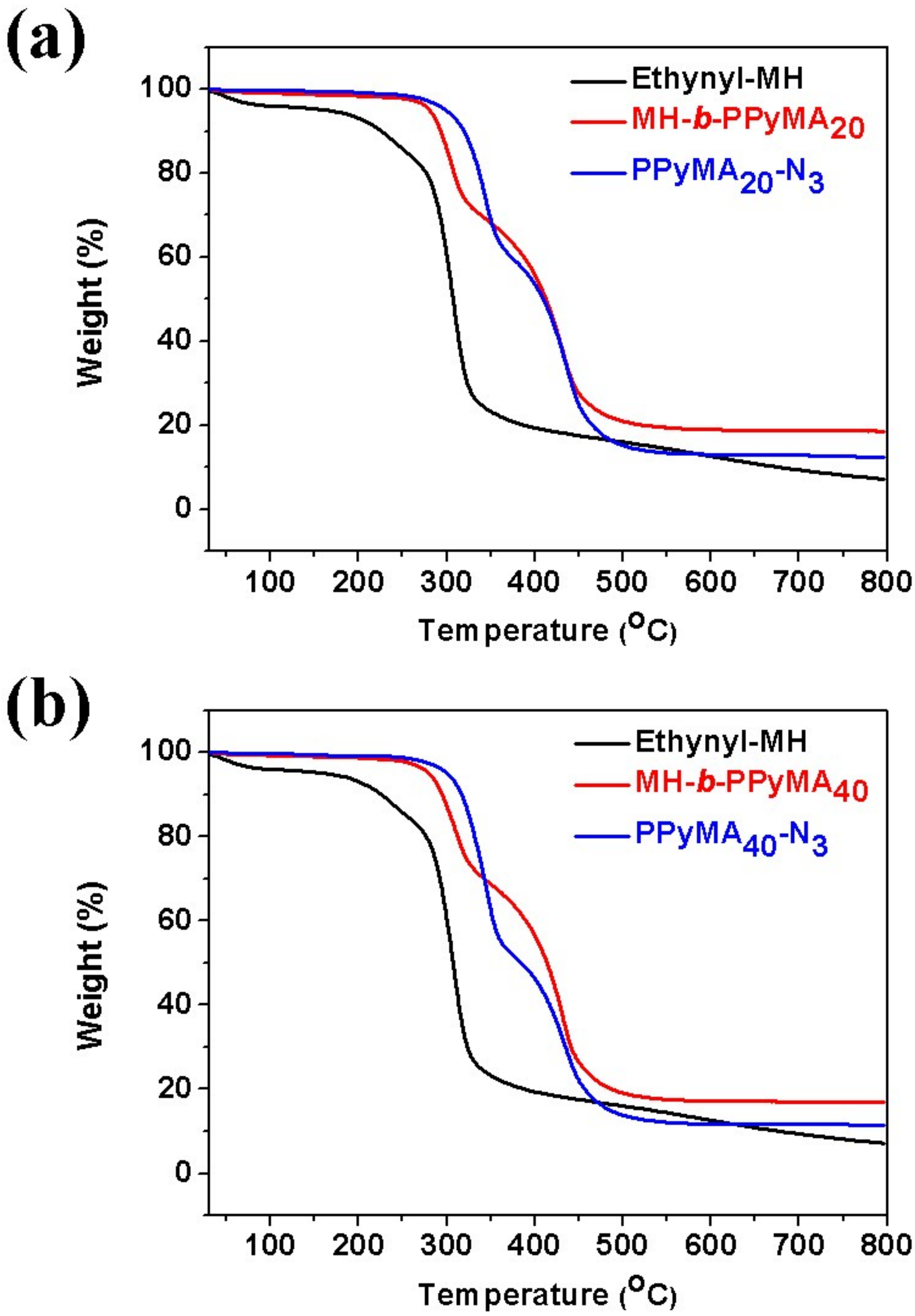

Fig. S7 TGA diagrams of (a) the ethynyl end-functionalized MH, azido-terminated $PPyMA_{20}$ homopolymer, and MH-*b*-$PPyMA_{20}$ block copolymer, and (b) the ethynyl end-functionalzed MH, azido-terminated $PPyMA_{40}$ homopolymer, and MH-*b*-$PPyMA_{40}$ block copolymer.

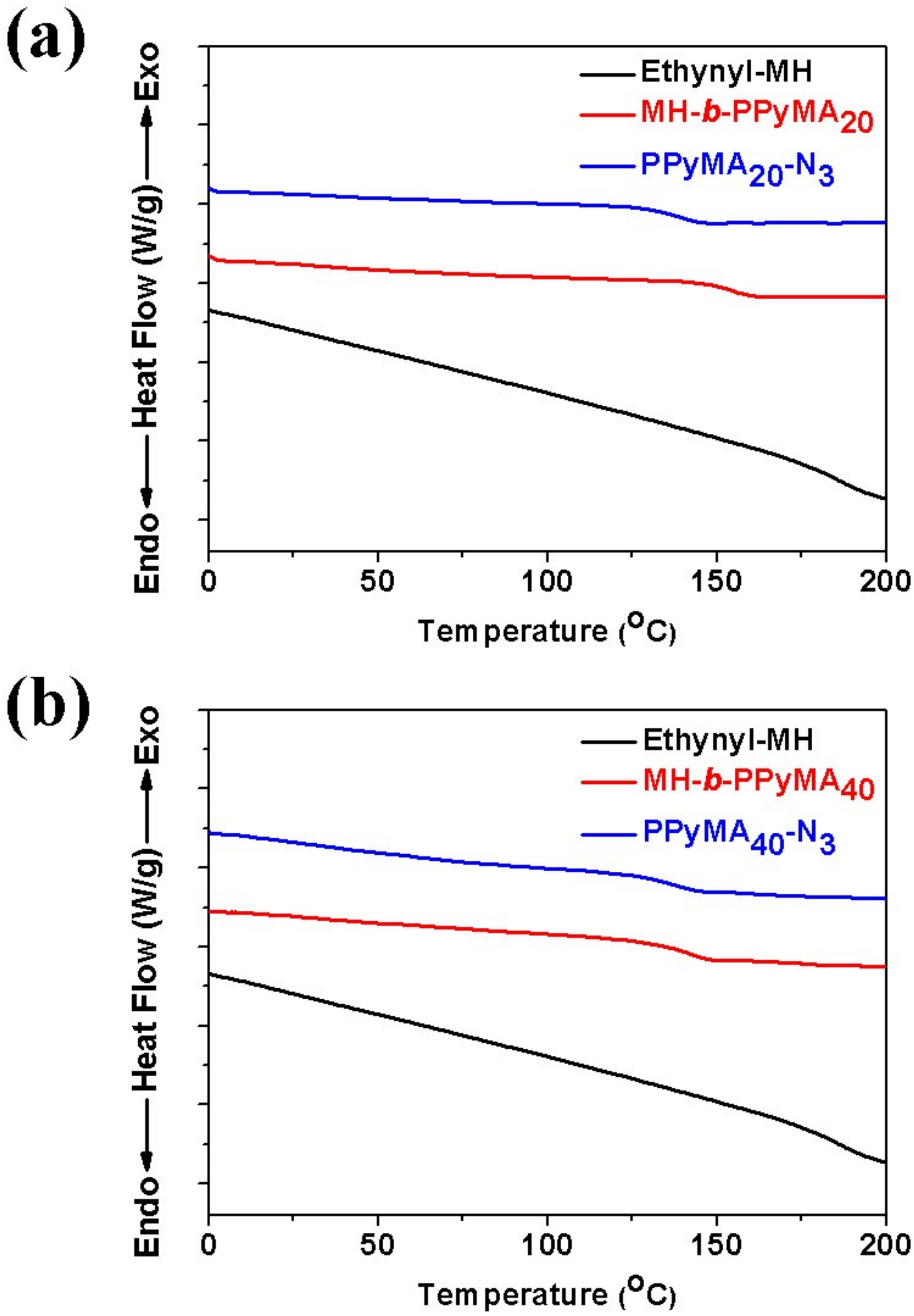

Fig. S8 DSC curves of (a) ethynyl end-functionalzed MH, azido-terminated $PPyMA_{20}$ homopolymer, and MH-*b*-$PPyMA_{20}$ block copolymer, and (b) the ethynyl end-functionalzed MH, azido-terminated $PPyMA_{40}$ homopolymer, and MH-*b*-$PPyMA_{40}$ block copolymer.

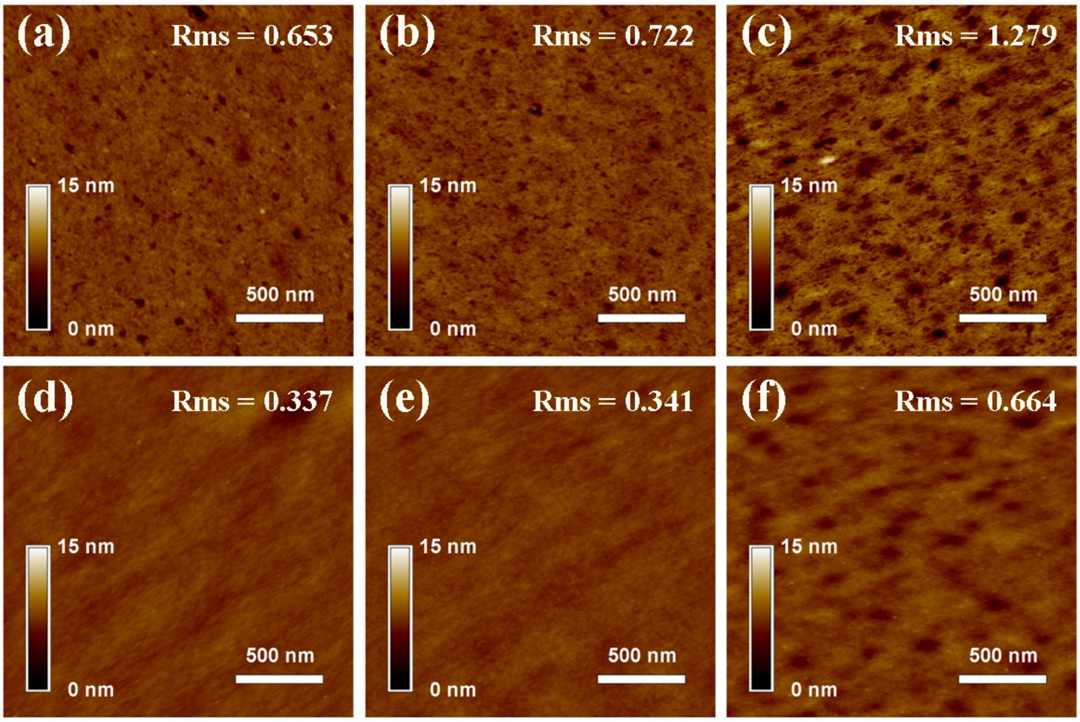

Fig. S9 AFM images of the surfaces of the MH-*b*-PPyMA$_n$ thin films: (a) as-cast MH-*b*-PPyMA$_{10}$ thin film, (b) as-cast MH-*b*-PPyMA$_{20}$ thin film, (c) as-cast MH-*b*-PPyMA$_{40}$ thin film, (d) thermo-annealed MH-*b*-PPyMA$_{10}$ thin film, (e) MH-*b*-PPyMA$_{20}$ thin film, and (f) MH-*b*-PPyMA$_{40}$ thin film.

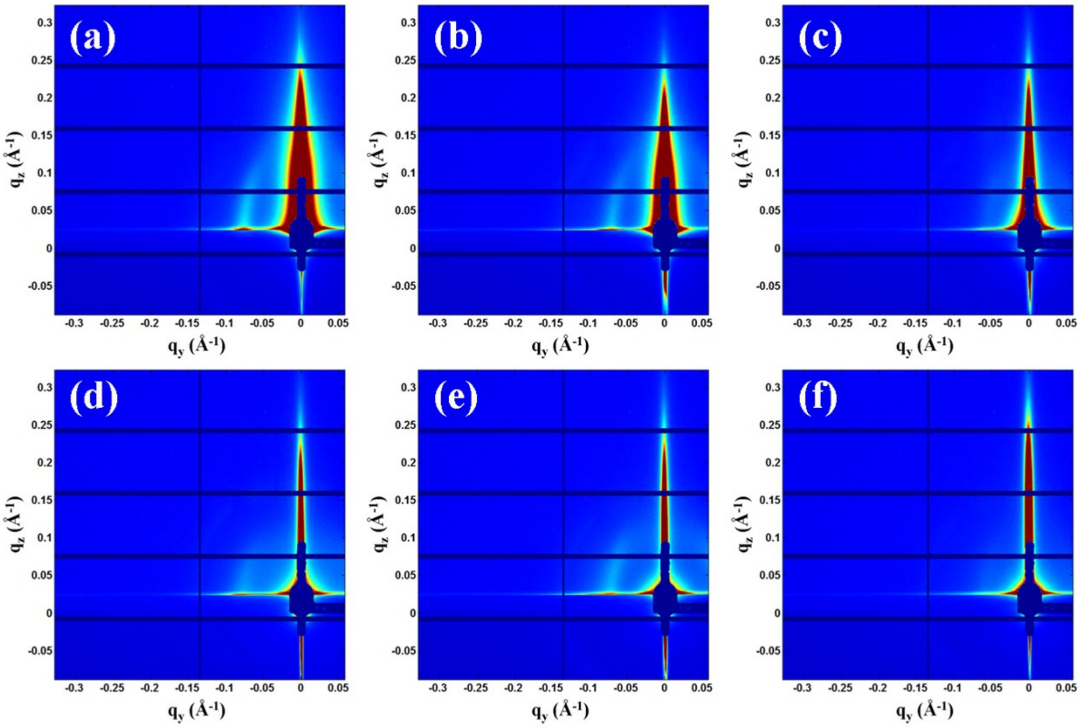

Fig. S10 2-D GISAXS patterns of the MH-*b*-PPyMA$_n$ thin films: (a) as-cast MH-*b*-PPyMA$_{10}$ thin film, (b) as-cast MH-*b*-PPyMA$_{20}$ thin film, (c) as-cast MH-*b*-PPyMA$_{40}$ thin film, (d) thermo-annealed MH-*b*-PPyMA$_{10}$ thin film, (e) MH-*b*-PPyMA$_{20}$ thin film, and (f) MH-*b*-PPyMA$_{40}$ thin film.

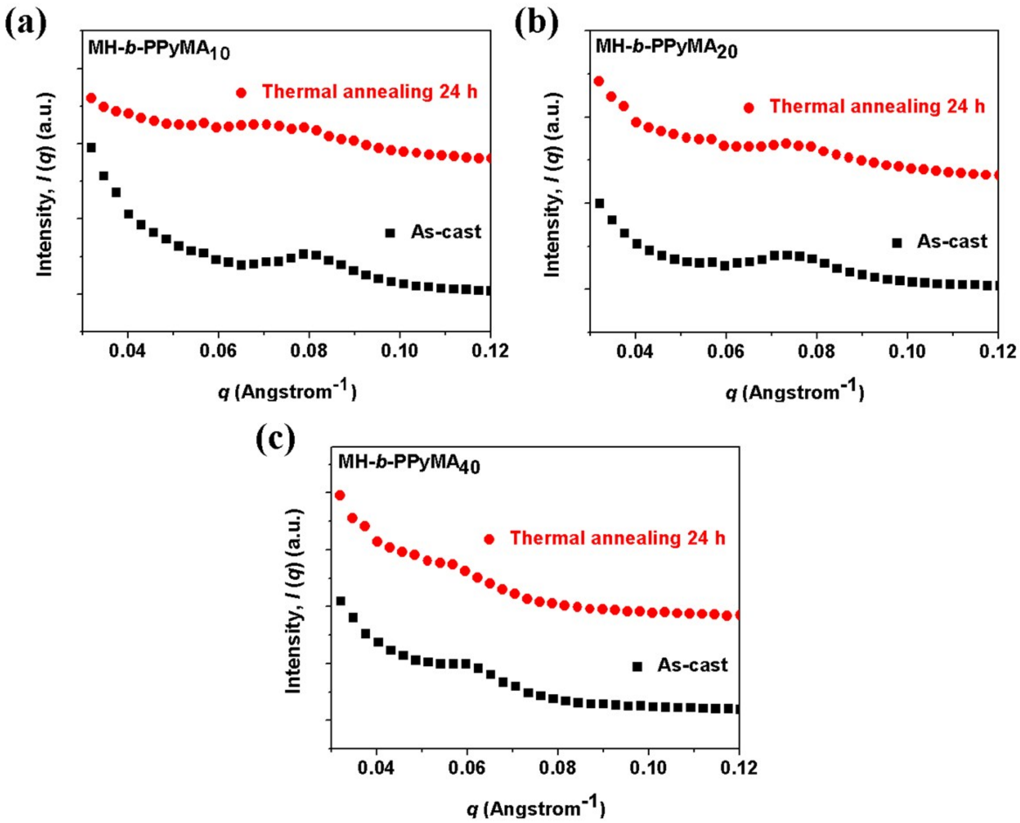

Fig. S11 1-D GISAXS q_y scanning plots of as-cast and thermo-annealed MH-*b*-PPyMA$_n$ thin films: (a) MH-*b*-PPyMA$_{10}$, (b) MH-*b*-PPyMA$_{20}$ and (c) MH-*b*-PPyMA$_{40}$.

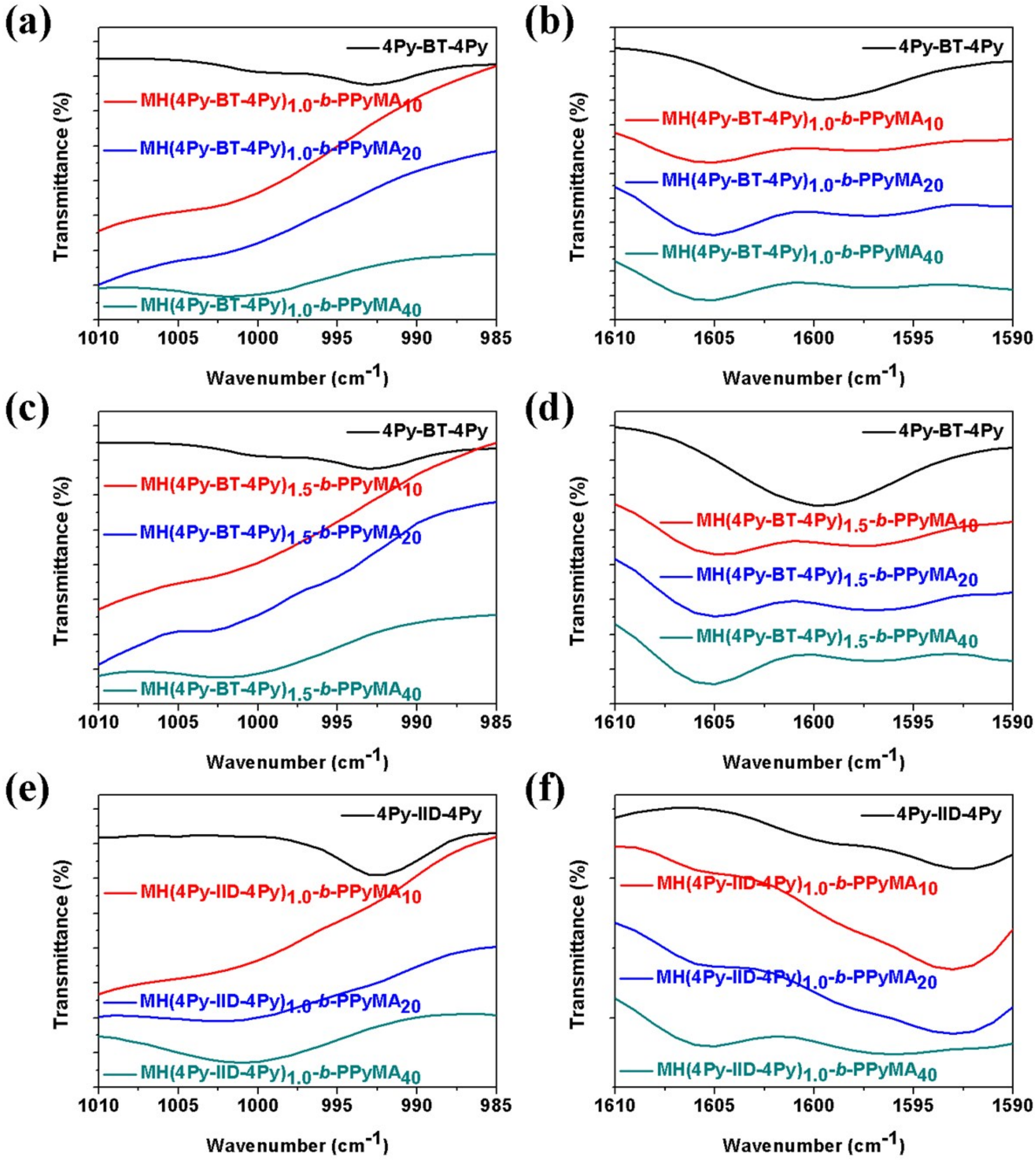

Fig. S12 FTIR spectra of MH(4Py-Acceptor-4Py)$_x$-*b*-PPyMA$_n$ supramolecular thin films: (a) and (b), MH(4Py-BT-4Py)$_{1.0}$-*b*-PPyMA$_n$; (c) and (d), MH(4Py-BT-4Py)$_{1.5}$-*b*-PPyMA$_n$; (e) and (f), MH(4Py-IID-4Py)$_{1.0}$-*b*-PPyMA$_n$.

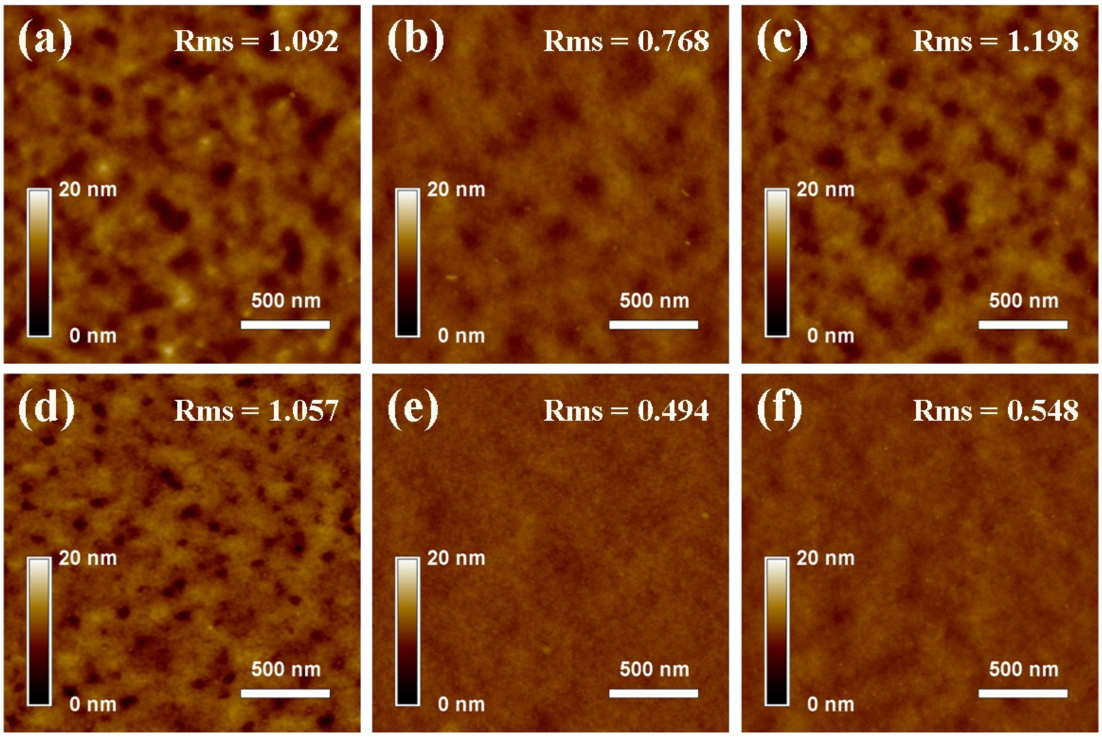

Fig. S13 AFM images of the surfaces of the thermo-annealed MH(4Py-Acceptor-4Py)$_x$-*b*-PPyMA$_n$ thin films (electret layers): (a) MH(4Py-BT-4Py)$_{1.5}$-*b*-PPyMA$_{10}$, (b) MH(4Py-BT-4Py)$_{1.5}$-*b*-PPyMA$_{20}$, (c) MH(4Py-BT-4Py)$_{1.5}$-*b*-PPyMA$_{40}$, (d) MH(4Py-IID-4Py)$_{1.0}$-*b*-PPyMA$_{10}$, (e) MH(4Py-IID-4Py)$_{1.0}$-*b*-PPyMA$_{20}$, and (f) MH(4Py-IID-4Py)$_{1.0}$-*b*-PPyMA$_{40}$.

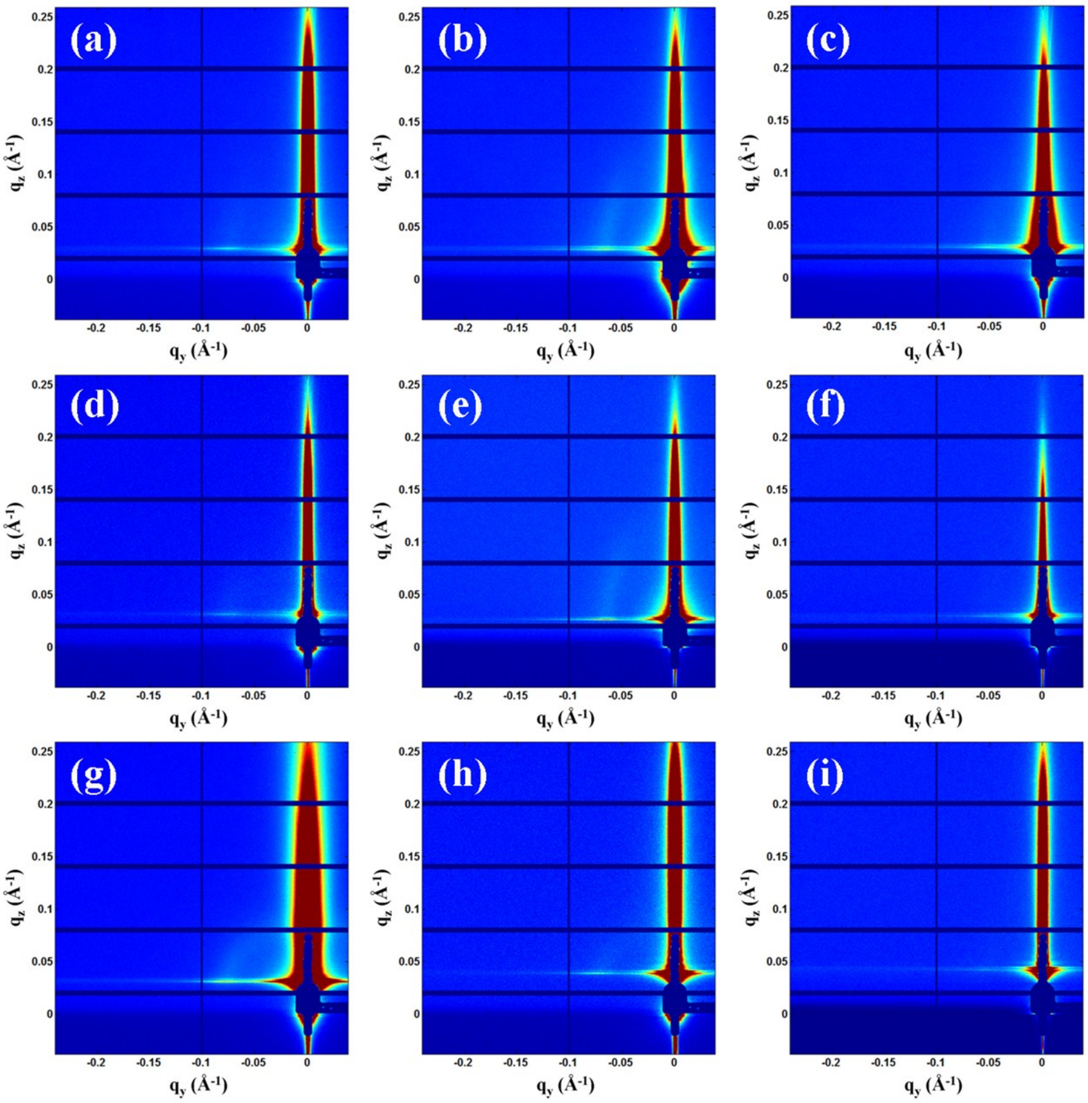

Fig. S14 2-D GISAXS patterns of the thermo-annealed MH(4Py-Acceptor-4Py)$_x$-*b*-PPyMA$_n$ thin films: (a) MH(4Py-BT-4Py)$_{1.0}$-*b*-PPyMA$_{10}$, (b) MH(4Py-BT-4Py)$_{1.0}$-*b*-PPyMA$_{20}$, (c) MH(4Py-BT-4Py)$_{1.0}$-*b*-PPyMA$_{40}$, (d) MH(4Py-BT-4Py)$_{1.5}$-*b*-PPyMA$_{10}$, (e) MH(4Py-BT-4Py)$_{1.5}$-*b*-PPyMA$_{20}$, (f) MH(4Py-BT-4Py)$_{1.5}$-*b*-PPyMA$_{40}$, (g) MH(4Py-IID-4Py)$_{1.0}$-*b*-PPyMA$_{10}$, (h) MH(4Py-IID-4Py)$_{1.0}$-*b*-PPyMA$_{20}$, and (i) MH(4Py-IID-4Py)$_{1.0}$-*b*-PPyMA$_{40}$.

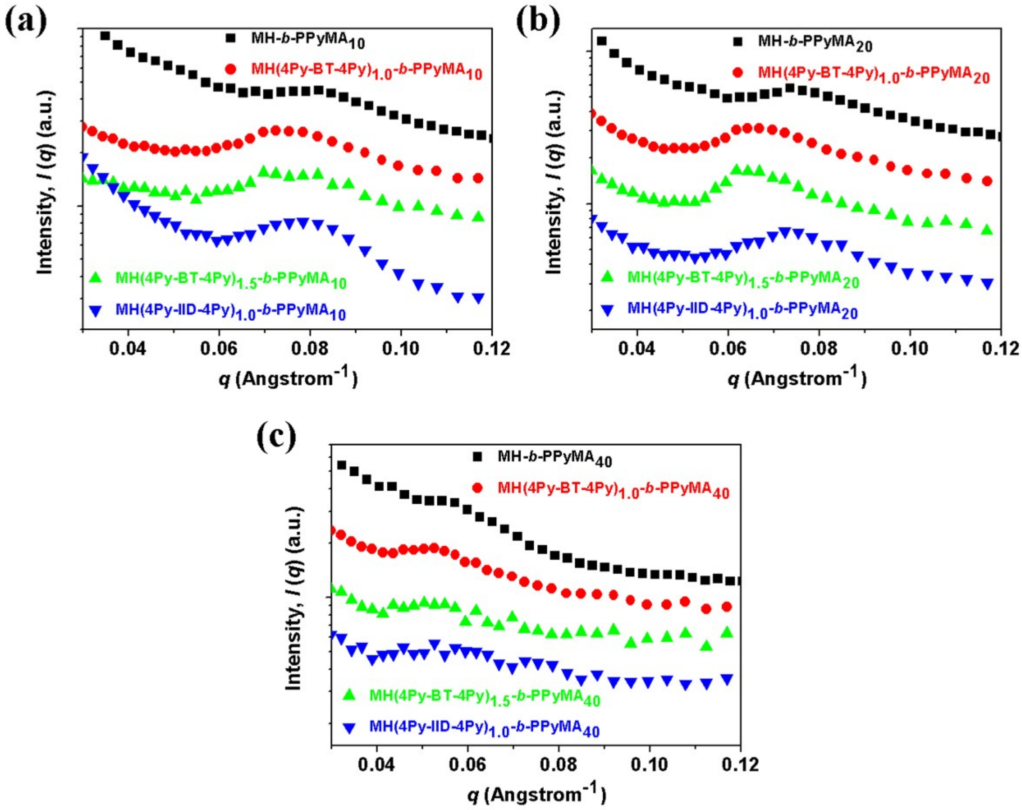

Fig. S15 1-D GISAXS q_y scanning plots of MH(4Py-Acceptor-4Py)$_x$-*b*-PPyMA$_n$ thin films: (a) MH(4Py-Acceptor-4Py)$_x$-*b*-PPyMA$_{10}$, (b) MH(4Py-Acceptor-4Py)$_x$-*b*-PPyMA$_{20}$, and (c) MH(4Py-Acceptor-4Py)$_x$-*b*-PPyMA$_{40}$.

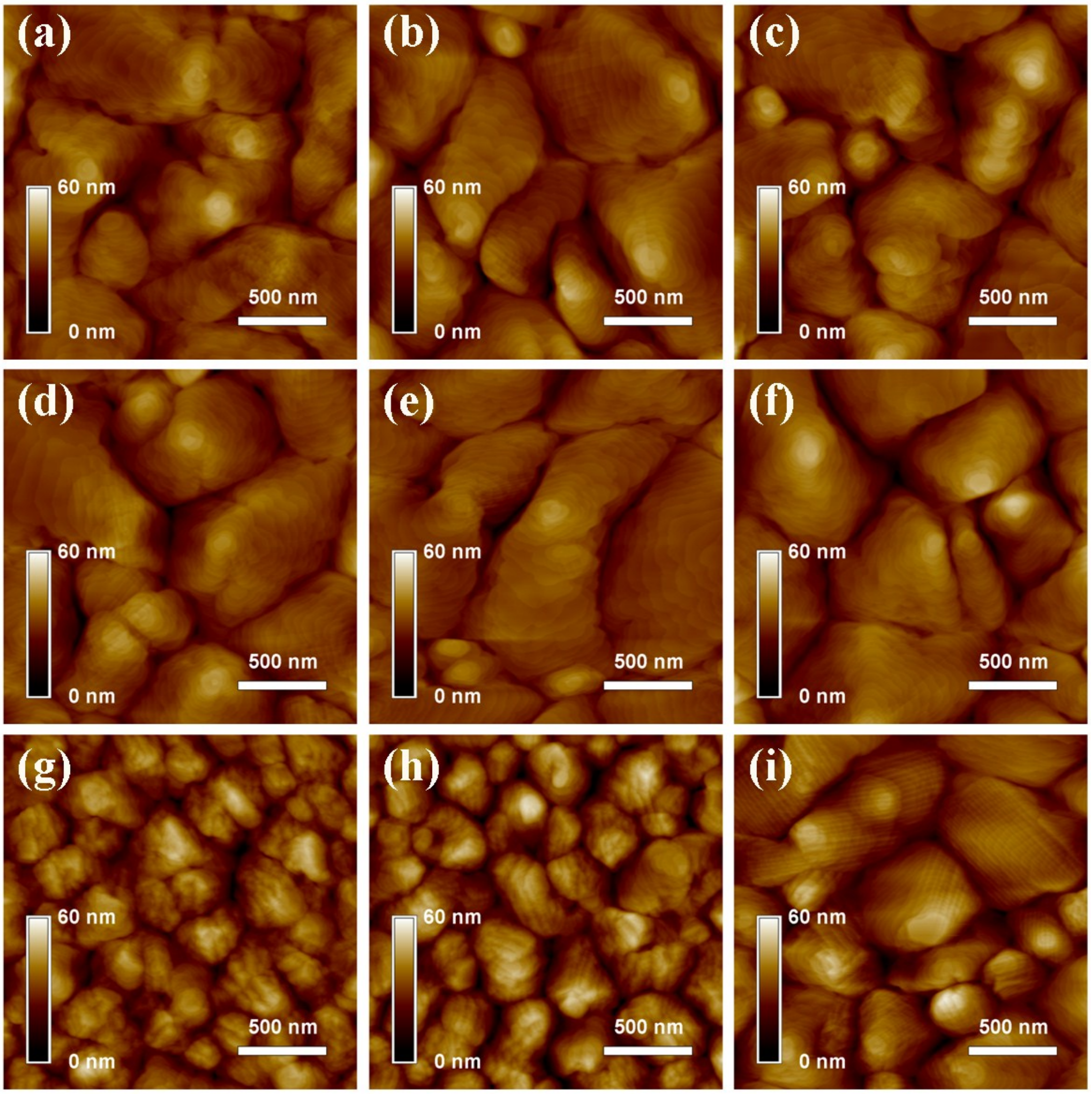

Fig. S16 AFM images of the surfaces of the pentacene layers grown from thermo-annealed MH(4Py-Acceptor-4Py)$_x$-*b*-PPyMA$_n$ thin films (electret layers): (a) MH(4Py-BT-4Py)$_{1.0}$-*b*-PPyMA$_{10}$, (b) MH(4Py-BT-4Py)$_{1.0}$-*b*-PPyMA$_{20}$, (c) MH(4Py-BT-4Py)$_{1.0}$-*b*-PPyMA$_{40}$, (d) MH(4Py-BT-4Py)$_{1.5}$-*b*-PPyMA$_{10}$, (e) MH(4Py-BT-4Py)$_{1.5}$-*b*-PPyMA$_{20}$, (f) MH(4Py-BT-4Py)$_{1.5}$-*b*-PPyMA$_{40}$, (g) MH(4Py-IID-4Py)$_{1.0}$-*b*-PPyMA$_{10}$, (h) MH(4Py-IID-4Py)$_{1.0}$-*b*-PPyMA$_{20}$, and (i) MH(4Py-IID-4Py)$_{1.0}$-*b*-PPyMA$_{40}$.

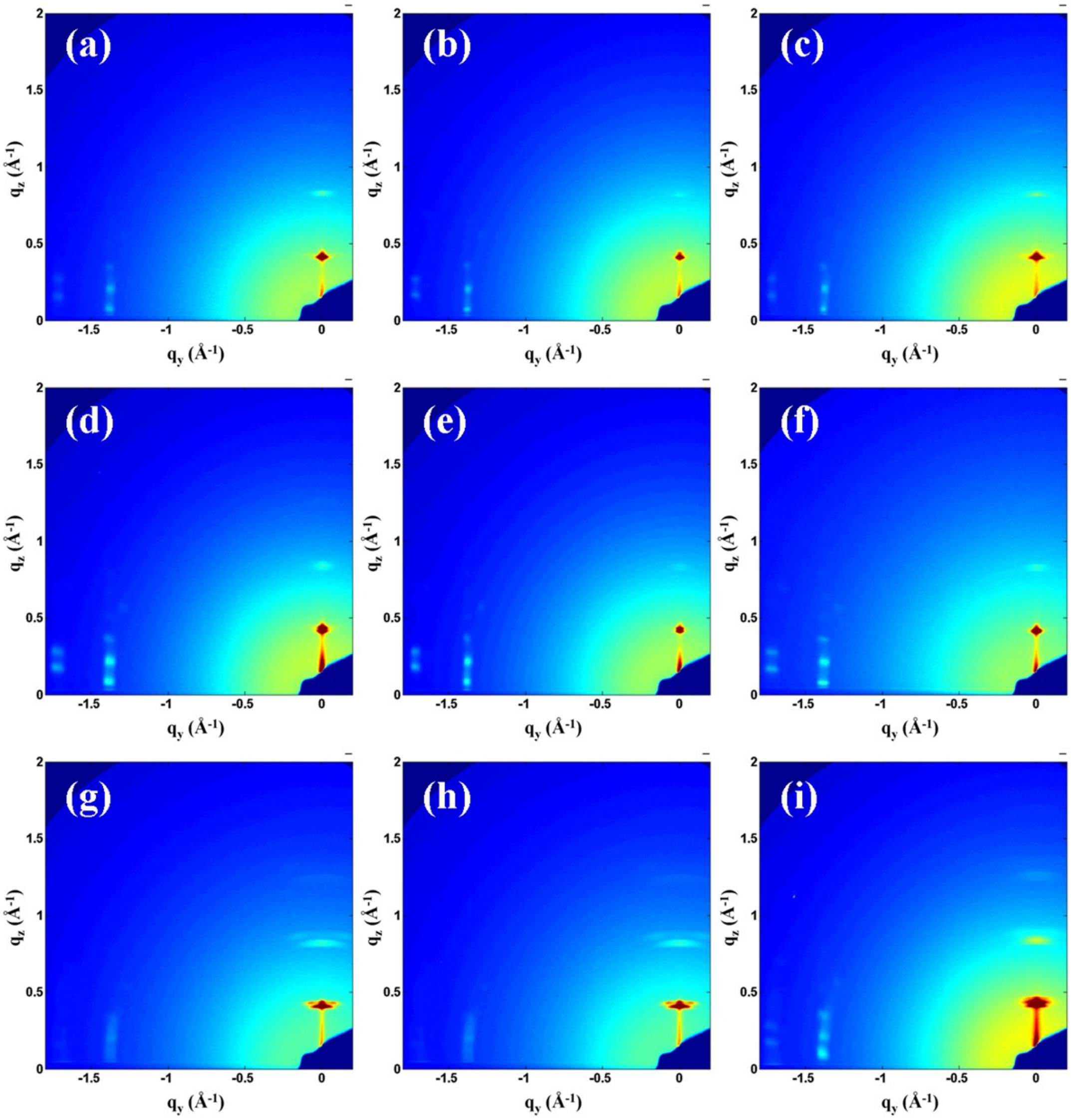

Fig. S17 2-D GIWAXS patterns of the pentacene layers grown from thermo-annealed MH(4Py-Acceptor-4Py)$_x$-*b*-PPyMA$_n$ thin films (electret layers) : (a) MH(4Py-BT-4Py)$_{1.0}$-*b*-PPyMA$_{10}$, (b) MH(4Py-BT-4Py)$_{1.0}$-*b*-PPyMA$_{20}$, (c) MH(4Py-BT-4Py)$_{1.0}$-*b*-PPyMA$_{40}$, (d) MH(4Py-BT-4Py)$_{1.5}$-*b*-PPyMA$_{10}$, (e) MH(4Py-BT-4Py)$_{1.5}$-*b*-PPyMA$_{20}$, (f) MH(4Py-BT-4Py)$_{1.5}$-*b*-PPyMA$_{40}$, (g) MH(4Py-IID-4Py)$_{1.0}$-*b*-PPyMA$_{10}$, (h) MH(4Py-IID-4Py)$_{1.0}$-*b*-PPyMA$_{20}$, and (i) MH(4Py-IID-4Py)$_{1.0}$-*b*-PPyMA$_{40}$.

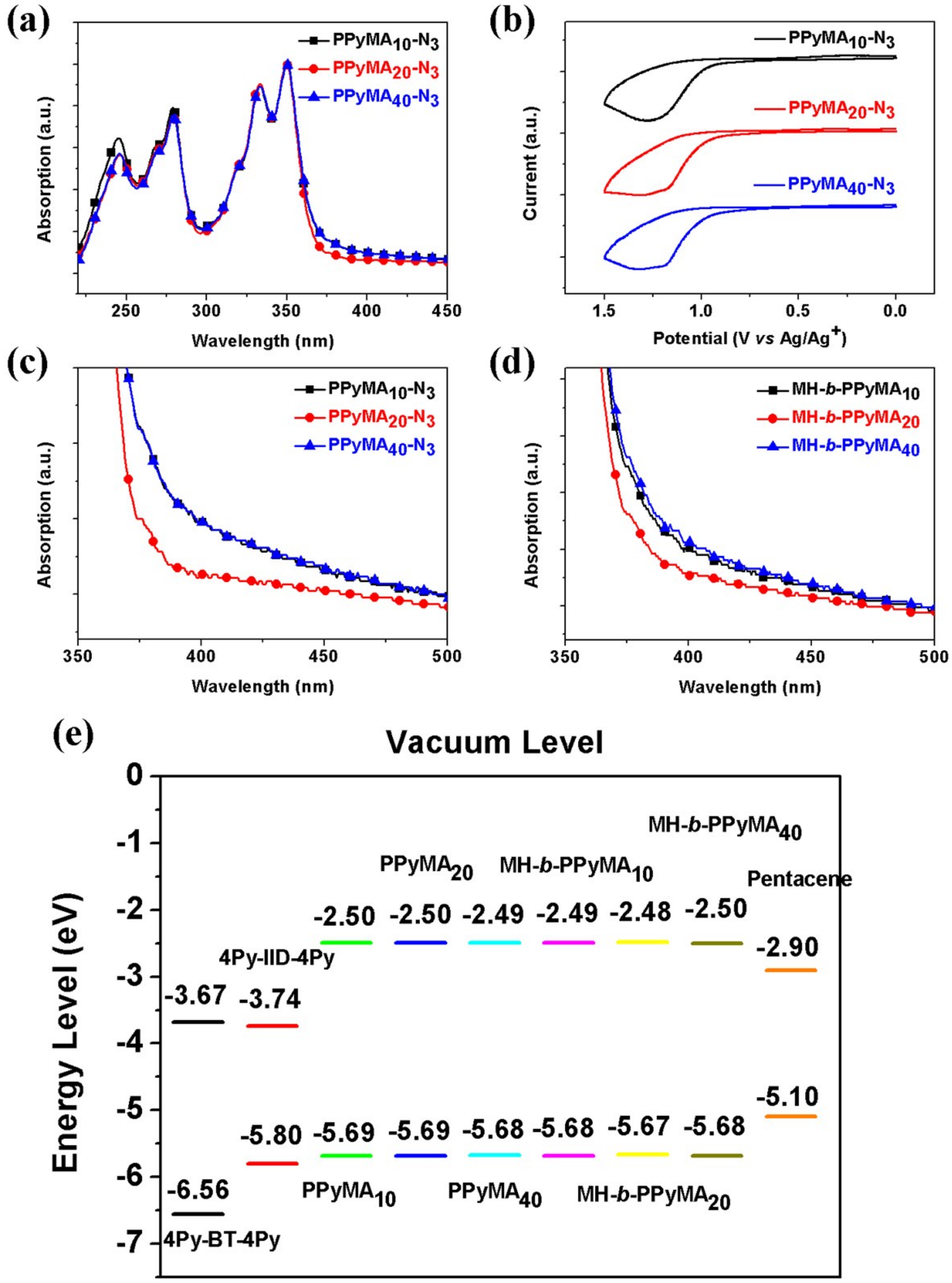

Fig. S18 (a) UV-Vis spectra of PPyMA$_n$-N$_3$ homopolymers in the region of 220 ~ 450 nm, (b) cyclic voltammograms of PPyMA$_n$-N$_3$ homopolymers, (c) UV-Vis spectra of PPyMA$_n$-N$_3$ homopolymers in the region of 350 ~ 500 nm, (d) UV-Vis spectra of MH-*b*-PPyMA$_n$ block copolymers in the region of 350 ~ 500 nm, and (e) energy levels of 4Py-Acceptor-4Py, PPyMA$_n$-N$_3$ homopolymers, MH-*b*-PPyMA$_n$ block copolymers, and pentacene.

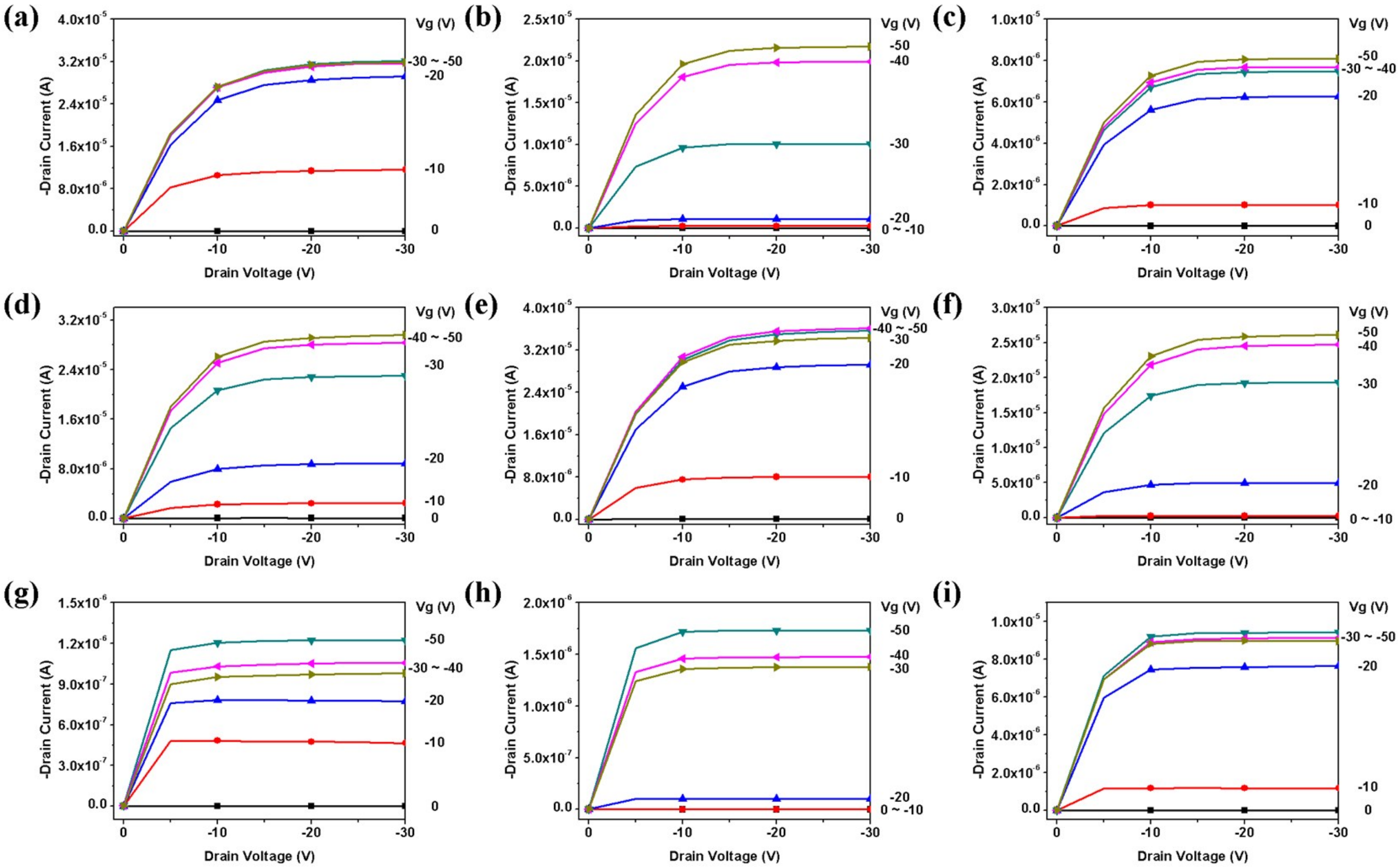

Fig. S19 The electric output curves of the devices using thermo-annealed MH(4Py-Acceptor-4Py)$_x$-*b*-PPyMA$_n$ thin films as electret layers: (a) MH(4Py-BT-4Py)$_{1.0}$-*b*-PPyMA$_{10}$, (b) MH(4Py-BT-4Py)$_{1.0}$-*b*-PPyMA$_{20}$, (c) MH(4Py-BT-4Py)$_{1.0}$-*b*-PPyMA$_{40}$, (d) MH(4Py-BT-4Py)$_{1.5}$-*b*-PPyMA$_{10}$, (e) MH(4Py-BT-4Py)$_{1.5}$-*b*-PPyMA$_{20}$, (f) MH(4Py-BT-4Py)$_{1.5}$-*b*-PPyMA$_{40}$, (g) MH(4Py-IID-4Py)$_{1.0}$-*b*-PPyMA$_{10}$, (h) MH(4Py-IID-4Py)$_{1.0}$-*b*-PPyMA$_{20}$, and (i) MH(4Py-IID-4Py)$_{1.0}$-*b*-PPyMA$_{40}$.

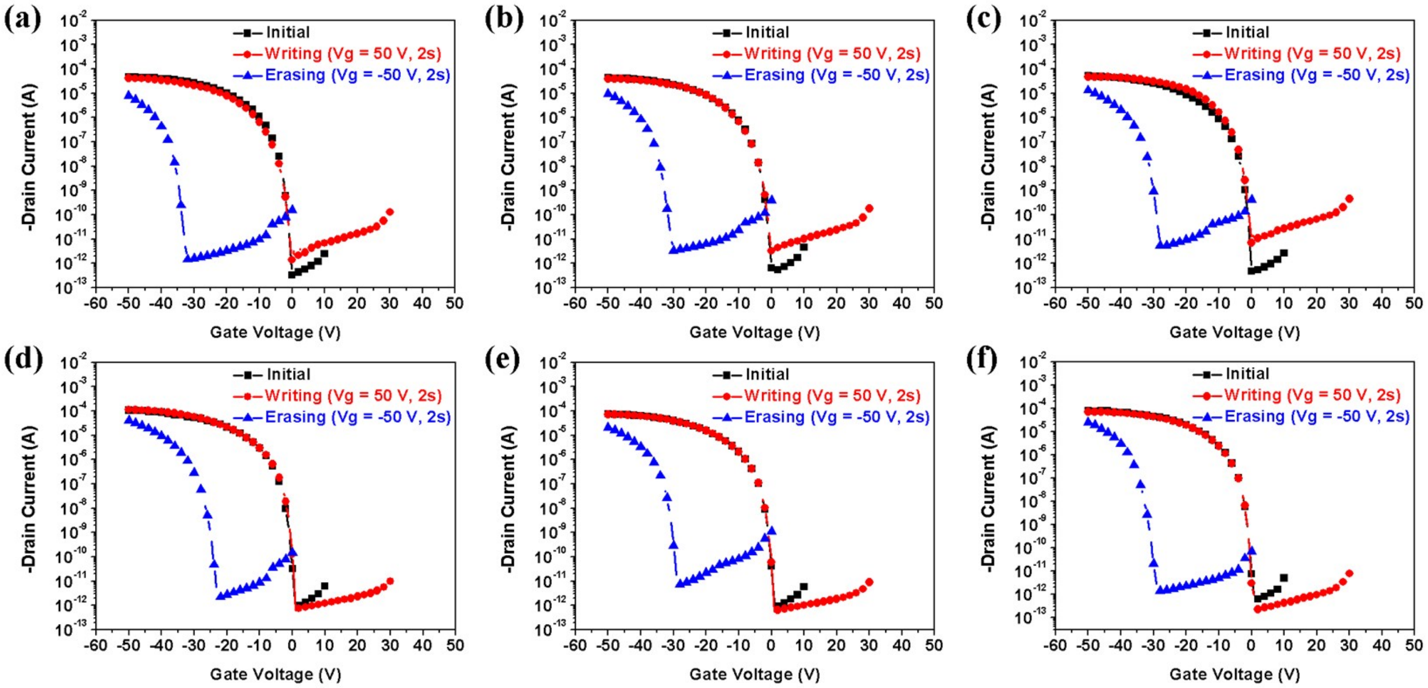

Fig. S20 The transfer curves of the devices using thermo-annealed PPyMA$_n$-N$_3$ and MH-*b*-PPyMA$_n$ thin films as electret layers: (a) PPyMA$_{10}$-N$_3$, (b) PPyMA$_{20}$-N$_3$, (c) PPyMA$_{40}$-N$_3$, (d) MH-*b*-PPyMA$_{10}$, (e) MH-*b*-PPyMA$_{20}$, and (f) MH-*b*-PPyMA$_{40}$.

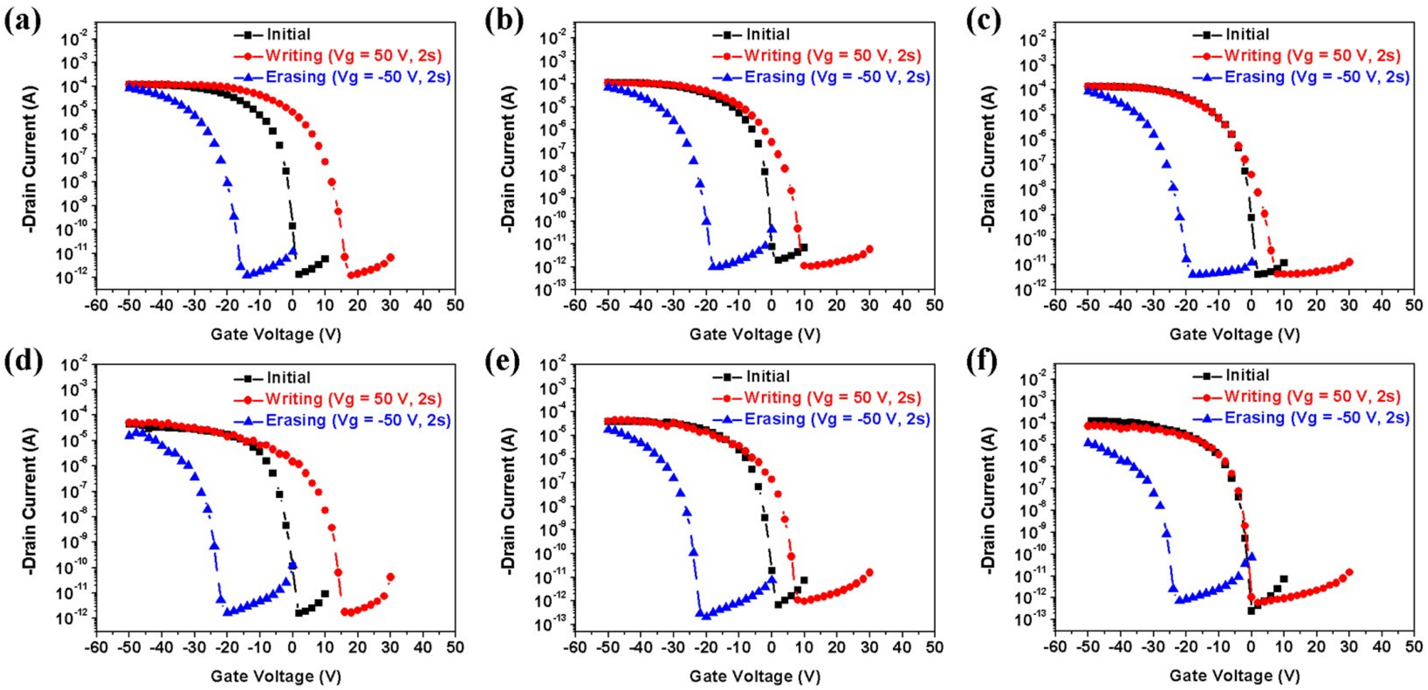

Fig. S21 The transfer curves of the devices using thermo-annealed MH(4Py-Acceptor-4Py)$_x$-*b*-PPyMA$_n$ thin films as electret layers: (a) MH(4Py-BT-4Py)$_{1.0}$-*b*-PPyMA$_{10}$, (b) MH(4Py-BT-4Py)$_{1.0}$-*b*-PPyMA$_{20}$, (c) MH(4Py-BT-4Py)$_{1.0}$-*b*-PPyMA$_{40}$, (d) MH(4Py-IID-4Py)$_{1.0}$-*b*-PPyMA$_{10}$, (e) MH(4Py-IID-4Py)$_{1.0}$-*b*-PPyMA$_{20}$, and (f) MH(4Py-IID-4Py)$_{1.0}$-*b*-PPyMA$_{40}$.

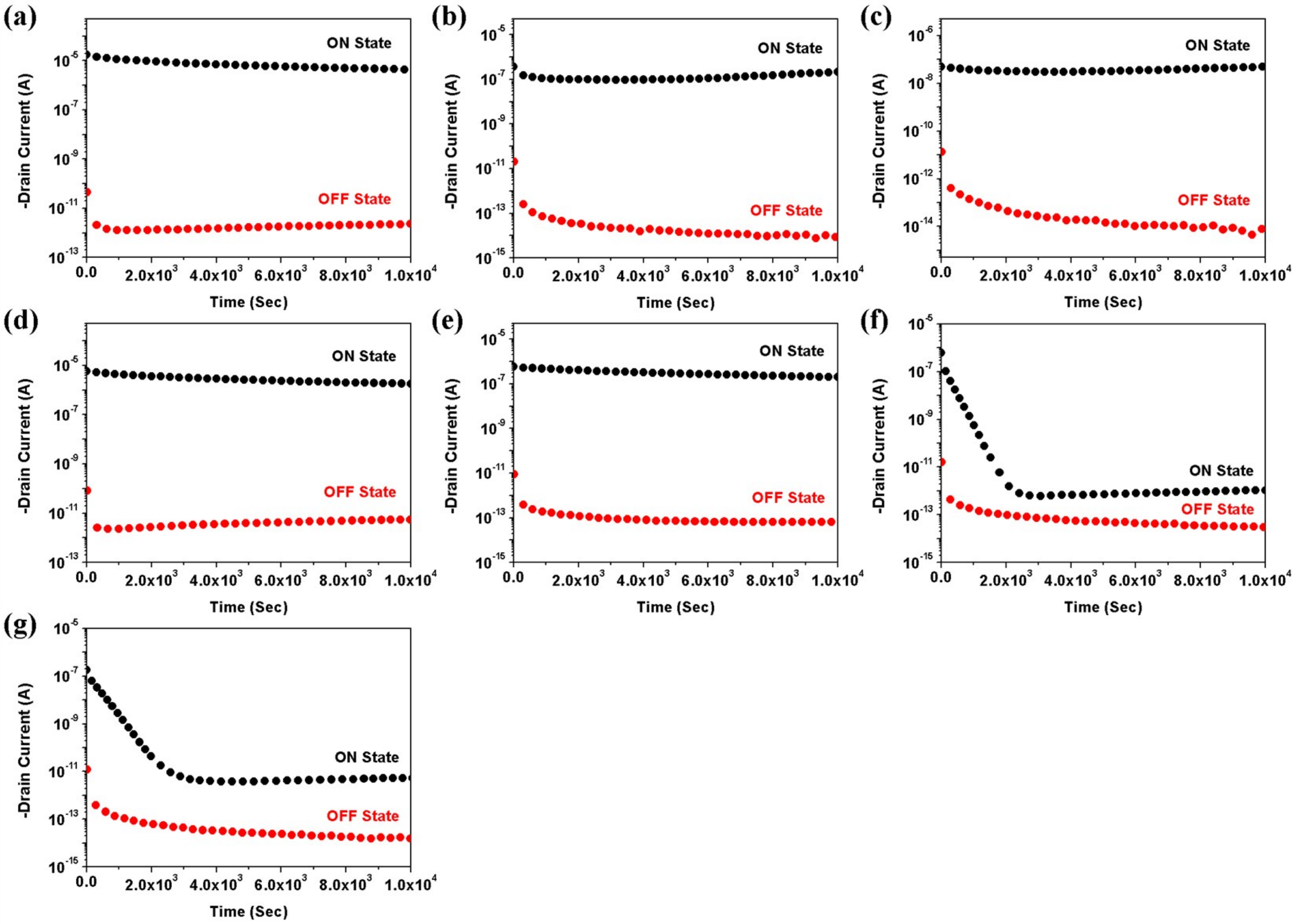

Fig. S22 The retention time curves of the devices using thermo-annealed MH(4Py-Acceptor-4Py)$_x$-*b*-PPyMA$_n$ thin films as electret layers: (a) MH(4Py-BT-4Py)$_{1.0}$-*b*-PPyMA$_{10}$, (b) MH(4Py-BT-4Py)$_{1.0}$-*b*-PPyMA$_{20}$, (c) MH(4Py-BT-4Py)$_{1.0}$-*b*-PPyMA$_{40}$, (d) MH(4Py-IID-4Py)$_{1.0}$-*b*-PPyMA$_{10}$, (e) MH(4Py-IID-4Py)$_{1.0}$-*b*-PPyMA$_{20}$, and (f) MH(4Py-IID-4Py)$_{1.0}$-*b*-PPyMA$_{40}$.

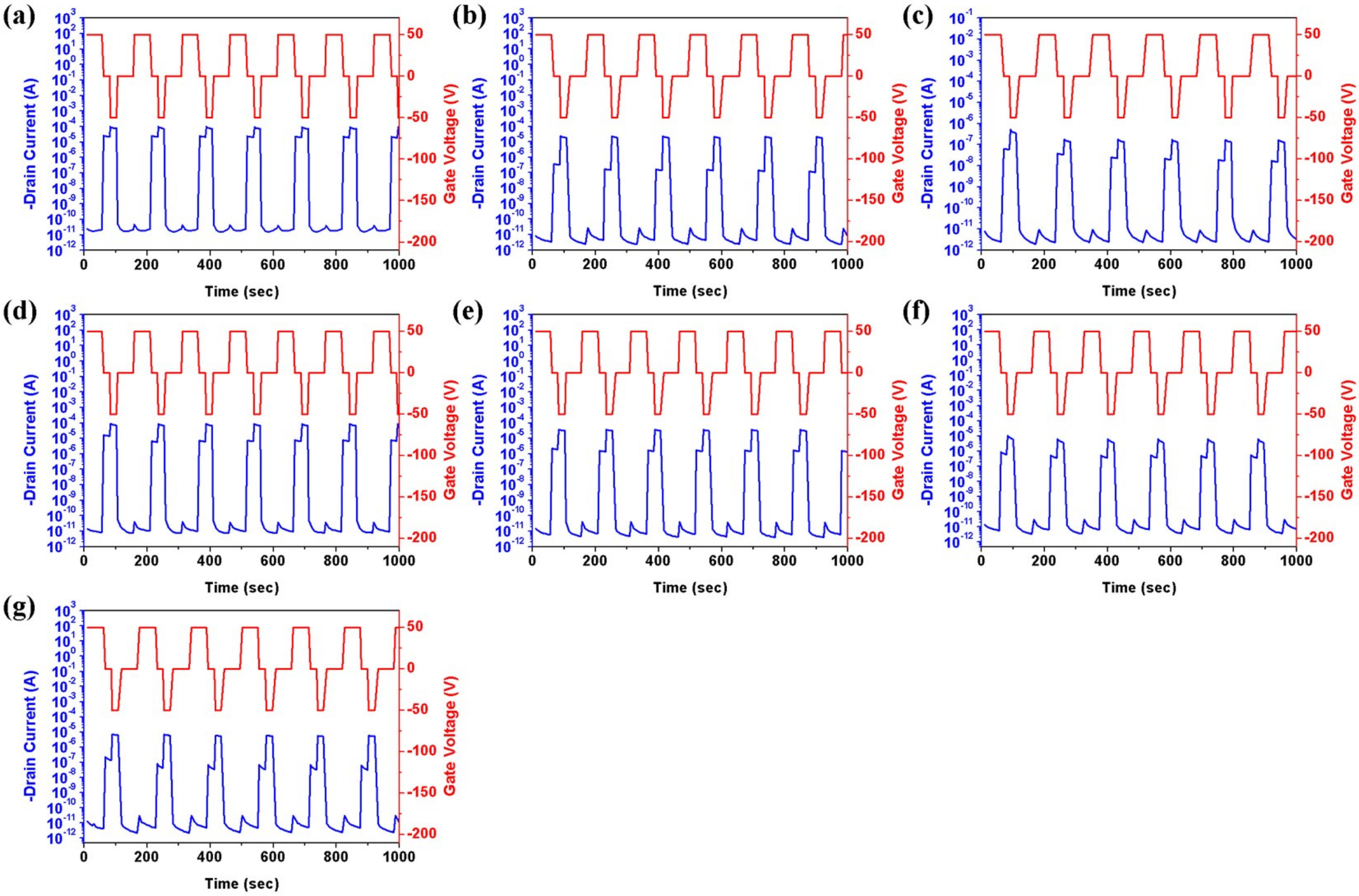

Fig. S23 The WRER (write-read-erase-read) cycles of the devices using thermo-annealed MH(4Py-Acceptor-4Py)$_x$-*b*-PPyMA$_n$ thin films as electret layers: (a) MH(4Py-BT-4Py)$_{1.0}$-*b*-PPyMA$_{10}$, (b) MH(4Py-BT-4Py)$_{1.0}$-*b*-PPyMA$_{20}$, (c) MH(4Py-BT-4Py)$_{1.0}$-*b*-PPyMA$_{40}$, (d) MH(4Py-IID-4Py)$_{1.0}$-*b*-PPyMA$_{10}$, (e) MH(4Py-IID-4Py)$_{1.0}$-*b*-PPyMA$_{20}$, and (f) MH(4Py-IID-4Py)$_{1.0}$-*b*-PPyMA$_{40}$.

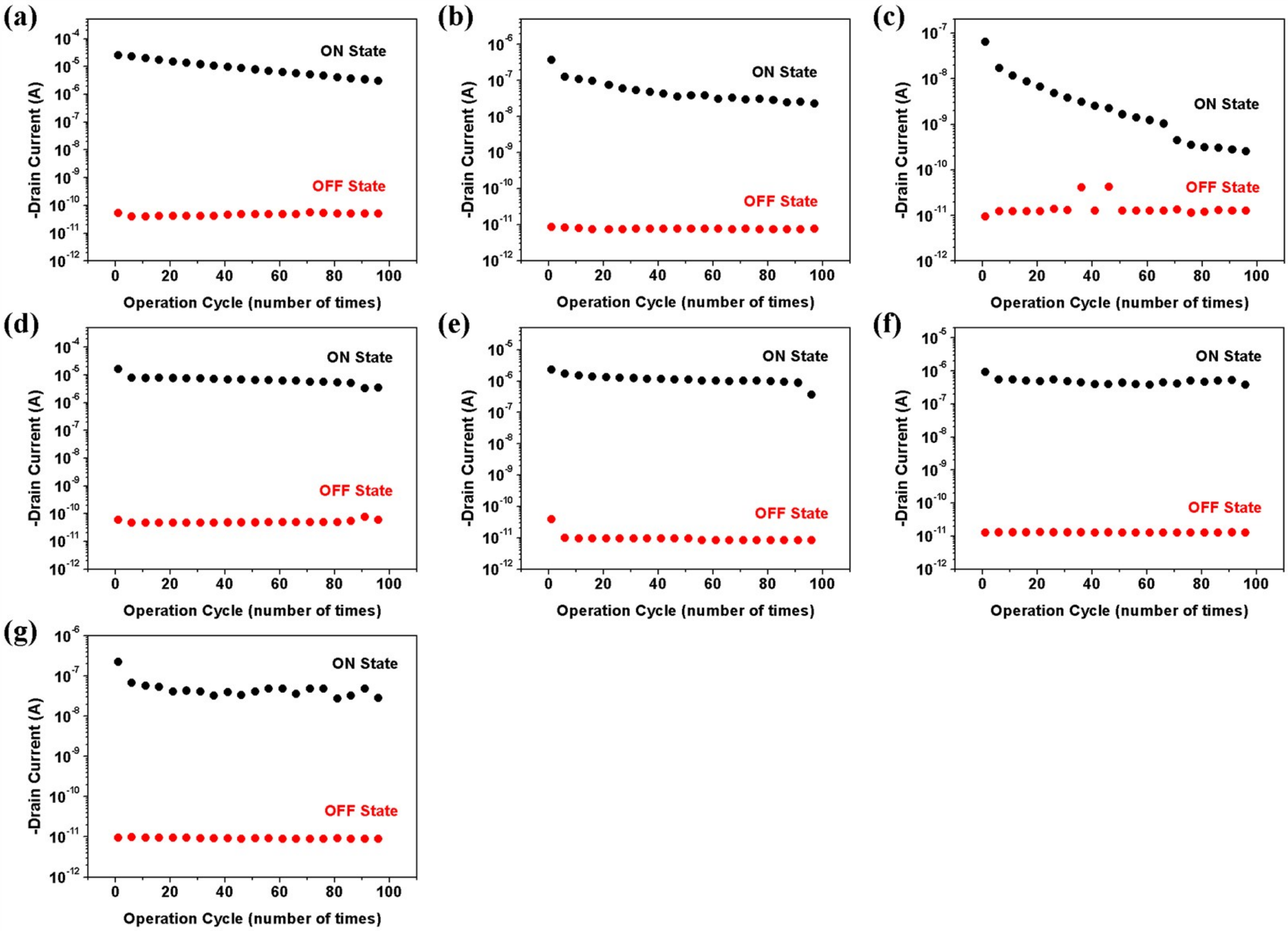

Fig. S24 The operation cycles (endurance) of the devices using thermo-annealed MH(4Py-Acceptor-4Py)$_x$-*b*-PPyMA$_n$ thin films as electret layers: (a) MH(4Py-BT-4Py)$_{1.0}$-*b*-PPyMA$_{10}$, (b) MH(4Py-BT-4Py)$_{1.0}$-*b*-PPyMA$_{20}$, (c) MH(4Py-BT-4Py)$_{1.0}$-*b*-PPyMA$_{40}$, (d) MH(4Py-IID-4Py)$_{1.0}$-*b*-PPyMA$_{10}$, (e) MH(4Py-IID-4Py)$_{1.0}$-*b*-PPyMA$_{20}$, and (f) MH(4Py-IID-4Py)$_{1.0}$-*b*-PPyMA$_{40}$.